Contents

1 Introduction

In this experiment, the linear relationship between beat frequency and angular velocity in a laser gyroscope is studied. First, the HeNe laser is set up on the turntable, etalon is used to generate a single mode beam. Using a smartphone, the turntable angular velocity settings are verified. Then, the beat frequency is recorded for different angular velocities. The β-factor, by which beat frequency and angular velocity are proportional, can then be determined using a linear fit. Finally, the lock-in limit can be observed and estimated.

2 Theory

In this section, a short introduction to the theoretical background necessary for this experiment will be given. Both the workings of a laser and the laser gyroscope and their limits the as well as the implementation and measurement of the beat frequency will be explained. If not specified otherwise, the information in this section is taken from [1] and [2].

2.1 Laser

Lasers are a source of coherent light, which means that the emitted light is monochromatic and in phase. It consists of three components. An active laser medium, a pumping mechanism to excite the medium, and a resonating cavity, which holds the active laser medium.

In quantum physics, only discrete energy values are allowed in atoms. When an atom is excited, it can relax into a lower energy state, and the excess energy is emitted. This is called spontaneous emission. If the energy is emitted as a photon, this photon will have a specific wave length due to the discrete energy levels. When an excited atom and a photon with the exact wave length that the atom emits when relaxing interact, the incoming photon can cause the atom to relax. Due to this process, a photon is emitted by the relaxing atom. This new photon has the same frequency, phase, polarization and direction of travel that the originally incoming photon has. This effect is called stimulated emission. If the two photons then interact with other excited atoms, stimulated emission occurs again and the light is amplified.

In a laser, this effect is used to produce coherent light. The active laser medium is excited by the pumping mechanism. Then, a spontaneous emission causes stimulated emission in the active laser medium. The active laser medium is placed in a resonating cavity, which is an arrangement of mirrors in which light of the desired wave length forms a standing wave. Thus, the light passes through the active laser medium several times, causing stimulated emission. At least one mirror must be partially transparent. The light can then leave the cavity through this mirror, and a laser beam is emitted.

However, to be able to consistently emit light, a population inversion must be maintained. This means that there must be more atoms that are excited than ground state atoms. Population inversion is a requirement for laser operation, as the light emitted by relaxing atoms are of exactly the frequency needed to excited the atoms. If there are more atoms in ground state, the light emitted by one atom will excite another atom. Only if population inversion is achieved, the rate of stimulated emission is higher than the rate of absorption, and there is a net light amplification.

When the atoms only transition between two energy states, lasting population inversion is not possible. Therefore, the atoms are often excited to a level that has a very fast, usually radiationless transition to a lower level that is not the ground state. Then, an atom from the lower level may decay to ground state by spontaneous emission, which then can cause stimulated transitions. If the lifetime of this transition is larger than the lifetime of the fast transition from the highest state to the lower level, the population of the highest state is essentially zero, and a population of atoms in the lower energy state will accumulate. Thus, a population inversion is achieved.

2.2 Helium Neon Laser

A Helium Neon laser (HeNe laser) is a laser that produces a continuous wave output. The active laser medium of a HeNe laser is a mixture of helium and neon gases. The helium is excited by an electrical discharge from ground state to its meta-stable 2^1S_0 and 2^3S_1 states. The excited helium atoms can only relax by collision with ground state neon atoms. The helium atoms then relax back to ground state, and the neon atoms are left in 3s and 2s states. The lower 2p state is not affected. The 3s and 2s state atoms then relax to 2p atoms, which in return transition by spontaneous emission to 1s state atoms. To maintain population inversion, the 1s neon atoms have to relax back to ground state. The 1s is a meta-stable state and the transition to ground state by optical emission is not allowed. However, the atoms can transition to ground state when energy is lost due to wall collisions. That is why in modern HeNe lasers the laser beam propagates through capillaries. In a HeNe laser, the main emission line of 632.8 nm is caused by the neon transition from 3s to 2p. The functionality of a HeNe laser is illustrated in fig. 1.

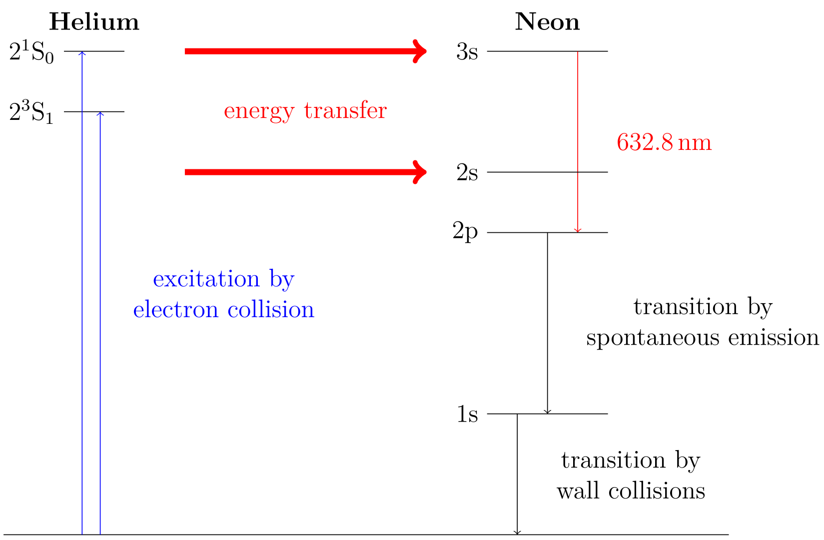

Figure 1: Sketch of the transitions relevant for the HeNe Laser (see [2]).

2.3 Sagnac Effect and Sagnac Interferometer

The Sagnac effect is a phenomenon encountered in rotating systems. Originally meant to test the theory of relativity, the Sagnac interferometer was used to study how electromagnetic radiation behaves in a rotating system.

The interferometer is placed onto a turntable. A coherent light beam is split by a beam splitter into a clockwise and counterclockwise beam. After one round trip, the beam is combined again by the beam splitter. The clockwise and counterclockwise beams experience a phase shift $\Delta\varphi$. It is proportional to the angular velocity ω of the turntable and is given by

$$\Delta\varphi = \frac{8 \cdot \pi}{\lambda c} \cdot \omega \cdot A \,, \tag{1}$$

where λ is the wave length of the light, c is the speed of light and A is the area enclosed by the light beam.

2.4 HeNe Ring Lase Gyroscope

In this experiment, an active laser gyroscope is used, with a HeNe laser as light source. It is different to a Sagnac interferometer in that the light source is not located outside the interferometer, instead, the active medium and resonating cavity are placed on the turntable. Three mirrors, placed in a equilateral triangle configuration, are used to keep the light on a triangular path. On one side, the active medium is placed. The setup is illustrated in fig. 2.

The mirror M_3, which is opposite of the active medium, is a curved mirror, while the other mirrors are flat. This is done because it is very hard to keep the light in the cavity. The curvature of the mirror allows for a redirection of escaping photons. To ensure optical stability of the three mirror ring resonator, the curvature R must fulfill the condition

$$\frac{R}{2} \leq d \leq R \tag{2}$$

for a side length d of the triangle.

Resonator modes

In a laser, only light of a wave length that forms a standing wave in the resonating cavity can be emitted, as the other wave lengths experience destructive interference. For a closed loop cavity (as is the case here), this is the case if half of the wave length λ is a multiple integer n of the resonating cavity length L

$$n = \lambda \cdot L \,. \tag{3}$$

In this case, the standing wave has n nodes. The word *mode* is used to refer to possible standing electromagnetic waves in a system. A resonator has ranges of frequencies called free spectral range $\Delta\nu$ within which no modes exist. It can be calculated from eq. (3) with the relation $\nu = c/\lambda$

$$\Delta\nu = \nu(n+1) - \nu(n) = \frac{c}{L} \,. \tag{4}$$

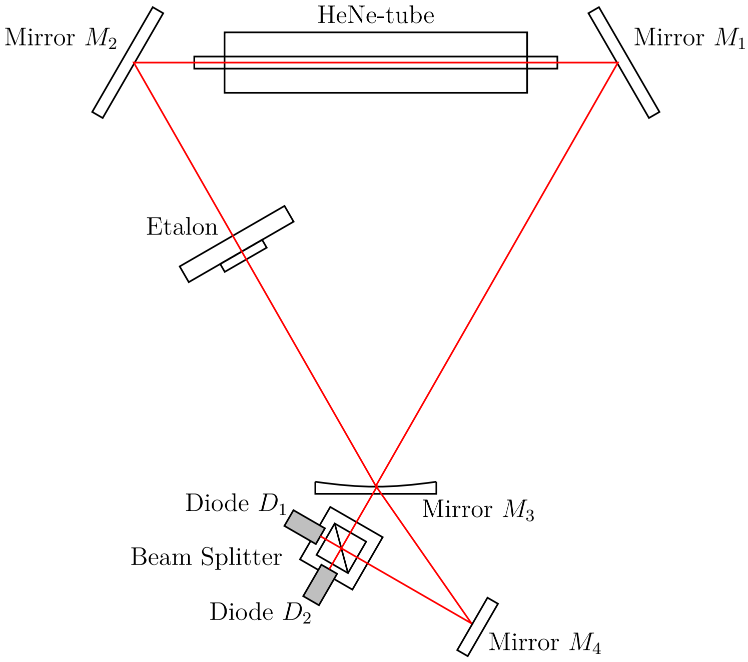

Figure 2: Sketch of the used setup. At the top, the HeNe tube can be seen. The mirrors M_1, M_2 and M_3 form the cavity. Mirrors M_1 and M_2 are flat while mirror M_3 is curved with a radius R. The single mode etalon is used to filter out exactly one mode. Behind mirror M_3, the clockwise and counterclockwise beams are separated and brought together by a beam splitter. Finally the superposed signals are examined using the diodes D_1 and D_2. If the whole apparatus is rotated with an angular velocity ω, the phase shift is examined using a comparator unit.

Usually, an electronic transition is accompanied by vibrational and rotational transitions. Therefore, the spectrum of the light emitted by the electronic neon transition described in section 2.2 is not discrete, but resembles a gaussian distrubution (pictured in fig. 3). As seen in fig. 3, there are a couple of resonator modes that fit under the neon gain profile.

Fabry-Perot-Etalon

For the ring laser gyroscope, only a single laser frequency should exist. A method of suppressing the undesirable modes is the use of etalon. Etalon is an optical resonator. It is a precisely ground glass cylinder with extremely parallel faces. The light that enters the etalon is partially reflected at the end. Inside the etalon, the light experiences interference with its reflection. The light of wave lengths that do not form a standing wave in the etalon experiences destructive interference and is therefore suppressed. Consequently, the transmissivity of etalon depends on the frequency and is maximized for the etalon modes. The width of the etalon is such that the maximum transmissivity corresponds to only one of the resonator modes. Thus, a single resonator mode is filtered.

In this experiment, the end faces are not coated, leading to a reflectivity of about 4 %. This is enough to provide a certain filter function and adds spectral losses.

The gain profile, the resonator modes and the etalon transmissivity is depicted in fig. 3.

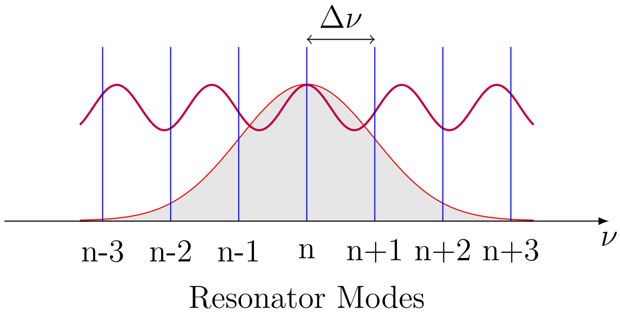

Figure 3: Sketch of the gain profile (red), resonator modes (blue) and etalon transmissivity (purple). Several resonator modes are possible within the gain profile of the laser. To extract exactly one mode, the width of etalon is selected to ensure low etalon transmissivity for all modes except for one.

Doppler Effect

The difference in frequency that the clockwise (cw) and counter clockwise (ccw) light beams experience can be explained by the Doppler effect. The source of photons is transitioning neon atoms, which emit light at a frequency of ν_0. If the atom is moving with a speed v, the frequency of the light ν shifts to

$$\nu = \nu_0 \left(1 + \frac{v}{c}\right) . \tag{5}$$

If the whole system is additionally rotating with an angular velocity of ω, the velocity due to the circular rotation v_{rot} is given by

$$v_{\text{rot}} = \omega \cdot r , \tag{6}$$

where r is the distance between atom and axis of rotation. Thus, the total velocity is given by the sum $v_{\text{tot}} = v + v_{\text{rot}}$ and the frequency of the light is given by

$$\nu_+ = \left(1 + \frac{v}{c} + \frac{\omega \cdot r}{c}\right) \qquad \nu_- = \left(1 - \frac{v}{c} - \frac{\omega \cdot r}{c}\right) . \tag{7}$$

In this case, ν_+ denotes the frequency of the light traveling in direction of rotation and ν_- the frequency of the light traveling against the direction of rotation.

The observed difference in frequency $\Delta\nu_{\text{tot}}$ is then given by

$$\Delta\nu_{\text{tot}} = \nu_+ - \nu_- = 2 \cdot \left(\frac{v}{c} + \frac{\omega \cdot r}{c}\right) , \tag{8}$$

and the difference in frequency caused by the rotation $\Delta\nu_{\text{rot}}$ is given by

$$\Delta\nu_{\text{rot}} = \nu_0 \frac{2 \cdot \omega \cdot r}{c} = \frac{4 \cdot F}{L \cdot \lambda}\omega =: \beta \cdot \omega , \tag{9}$$

using $F = 1/2 \cdot L_1 \cdot h$ and $L = L_1 + L_2 + L_3$. In this case, L_i are the side lengths of the triangle and h is the height of the triangle perpendicular to L_1.

2.5 Lock-In Effect

One limitation of the laser gyroscope is the so-called lock-in effect. It refers to the fact that for very low angular velocities, no frequency difference can be observed between the clockwise and counterclockwise beam. This is caused by weak mutual coupling of the clockwise and counterclockwise beam [3].

The coupling happens due to back-scattering of light at the mirrors and other optical components. For a scatterer of small dimensions compared to the wave length, the energy of the scattered light depends on the wave position, reaching its maximum at anti-nodes. Therefore, the energy loss one beam experiences depends on the relative phase of the other beam, which causes the coupling. For higher angular velocities, the difference in frequency for the standing waves is too high for the coupling to occur. For these angular velocities, the linear relationship derived in eq. (9) holds.

As a result, a laser gyroscope can not measure very low angular velocities, as for these the linear relationship between frequency difference and angular velocity is broken. The angular velocity at which the the lock-in effect can not be observed anymore is referred to as the *lock-in limit*.

As the back-scattering strongly depends on dust deposit and other contamination of the optical components, the directly correlated lock-in limit is not constant. It can be approximated by

$$\omega_{\text{Lock}} = \frac{c \cdot \lambda}{8 \cdot \pi \cdot F} \cdot \varepsilon \cdot \cos(\gamma)\,, \tag{10}$$

where γ is the back-scattering angle and ε is the back-scattering coefficient. Taking the worst case, where γ is $0°$, the back-scattering coefficient is about $\varepsilon = 10^{-4}$, an approximation for the lock-in limit is given by

$$\omega_{\text{Lock}} = \frac{c \cdot \lambda}{8 \cdot \pi \cdot F} \cdot 10^{-4}\,. \tag{11}$$

2.6 Measuring the Beat Frequency

When two waves with a very small difference in frequency interfere, the amplitude of the interference maxima of the resulting wave oscillates with the frequency difference of the original waves. This is the frequency that has to be measured to determine the difference in frequency of the original waves.

In the laser gyroscope, the beam splitter combines the clockwise and counter clockwise beam and splits them back up, so that 50 % of the combined beam reaches each photo diode. The photo diodes measure the intensity of the interference pattern, which oscillates with the beat frequency. The photo diodes are placed in such a way that the interference patterns they detect are phase shifted by 180°. The photo diode signals are then put on top of each other. To measure the beat frequency, a comparator is used. It outputs a logical signal which switches from zero to one and vice versa exactly when both photo diode signals have the same amplitude.

Ideally, the intensity measured by the photo diodes should reach zero, corresponding to 100 % interference contrast. However, in real applications the contrast is often lower. This is why the comparator is used to determine the beat frequency. As the logical signal changes when the photo diode amplitudes are the same, the comparator output is independent of the interference contrast and offset variations.

The photo diode signals and corresponding comparator outputs are depicted in fig. 4.

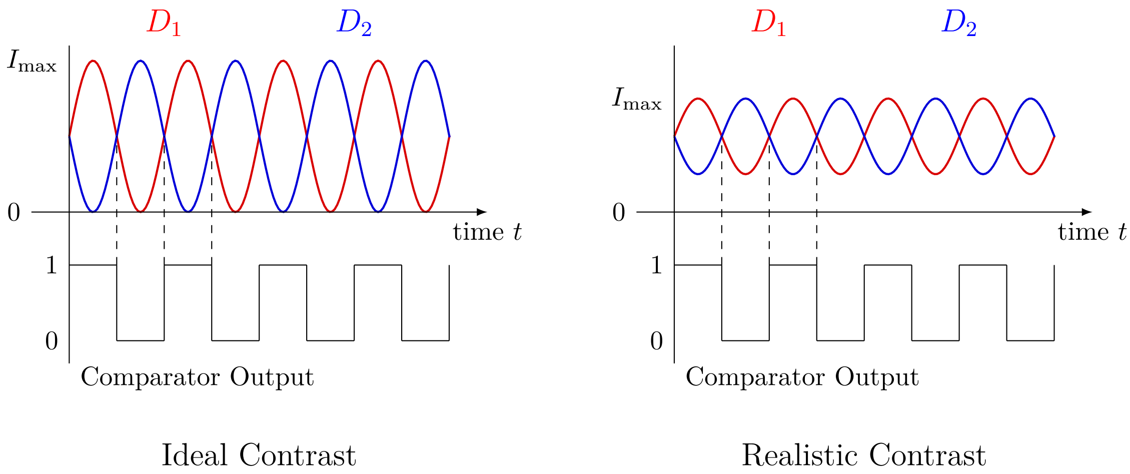

Figure 4: Comparator output depending on the photo diode signal. The signal of two photo diodes D_1 and D_2 is phase shifted by 180°. To measure the beat frequency, the comparator signal switches from one to zero and vice versa exactly when both photo diode signals have the same amplitude. When measuring this way, the comparator signal is not dependent on the interference contrast. For an ideal signal, pictured left, this method of measuring does not offer any advantage. However, in the realistic signal (pictured right), there is some noise and the intensity does not reach zero. Regardless, the comparator produces the desired result, identical to the ideal case.

3 Setup and Execution of the Experiment

In this experiment, an `eLas CA-1310` ring laser gyroscope is used. The full setup can be seen in figs. 12 and 13 and the schematic structure in fig. 2. The HeNe laser tube provides the pump energy and the active medium for the laser. The mirrors M_1 to M_3 form the cavity. The setup is placed on a turntable and operated using separate controllers for the laser and the stepper motor rotating the turntable. Readout electronics for the two photo diodes, an oscilloscope and a frequency counter are used to acquire the data.

A careful calibration of the cavity is necessary for the laser to work properly. In our case, the mirrors and the etalon were already perfectly aligned so that only small adjustments were necessary. If the setup would not have been calibrated, the following steps would have been taken to do so. First, the etalon is removed from the optical axis. Then, the green calibration laser is placed behind mirror M_1. It is then aligned in height and direction for the light beam to pass through the mirror and the HeNe tube. It can be observed on a piece of paper behind the HeNe tube. The position of the HeNe tube is adjusted until the light beam passes directly through the tube without any unwanted reflections. This is assured by adjusting the tubes height and rotation until a clear laser point is visible on the paper screen behind it. If distortions or multiple laser points are visible, the adjustments have to be optimized further. It should be tried to make the settings accordingly so that light beam hits mirror M_2 directly at the center. After adjusting the HeNe tube, mirror M_2 is tilted until the light beam hits mirror M_3 and will not change in height while passing the optical axis. The same adjustments are then made for mirror M_3 until the light hits mirror M_1 again. It it now important that the light beam hits exactly the same position on M_1 as before. This is guaranteed by watching the transmission behind mirror M_1. Several meters behind the mirror, the light beam can be seen as a reflection on the wall. The tilting of the mirrors has now to be adjusted until the reflection is as clear and point-shaped as possible, as this allows to extrapolate the course of the light beam after passing the ring cavity many times. If for example a line is visible instead of a point shape, this means that the beam changes its height while passing the optical axis. The mirrors have to be adjusted accordingly so that this does not happen. If the mirrors have been aligned correctly, the HeNe laser can now be turned on and the green calibration laser can be removed.

From this point on, the further calibrations were also performed during this experiment. The alignment of the mirrors and the HeNe tube was already sufficient.

Next, the single mode etalon was mounted between mirrors M_2 and M_3. After assuring that it was not tilted in respect to the incoming light beam, it was rotated until the laser was strong enough to see transmissions behind all mirrors, visible as reflections from the walls (see fig. 13). Now, the beam behind mirror M_3 is examined. To do so, diode D_2 was removed and the light beam after the beam splitter was examined. First it was assured that the superposed light beam appeared as a clear spot directly behind the beam splitter. Mirror M_4 was adjusted until this was reached. After that, the light beam at a certain distance, approximately 3 m, was examined and the beam splitter itself was tilted until a clear beam profile was visible. If it was tilted too far in one direction, two spots appeared instead of one, resulting from the clockwise and counterclockwise propagating beams. These calibration steps can be seen in figs. 14 and 15. Only if the light beam close to and far from the beam splitter appeared as a single peak, it can be assured that the two beams were rejoined correctly in the beam splitter to get the maximum interference later.

After placing diode D_2 behind the beam splitter again, the signals could be observed on the oscilloscope. As the cavity is very sensitive to vibrations, a lot of noise could be seen by just tapping on the table. As the signals of the photo diodes should have a final phase shift of 180° for correct use of the comparator and frequency counter unit, it was checked on the oscilloscope. In the optimal case, these noisy signals should have exactly the expected phase shift. A signal of the noisy intensities on the oscilloscope can be seen in fig. 5.

Already, a phase shift of around 180° can be estimated. To get a clearer signal for better comparability of clockwise and counterclockwise signal, a stimulated vibration was tried to achieve by placing a smartphone on the turntable and playing sound with a certain

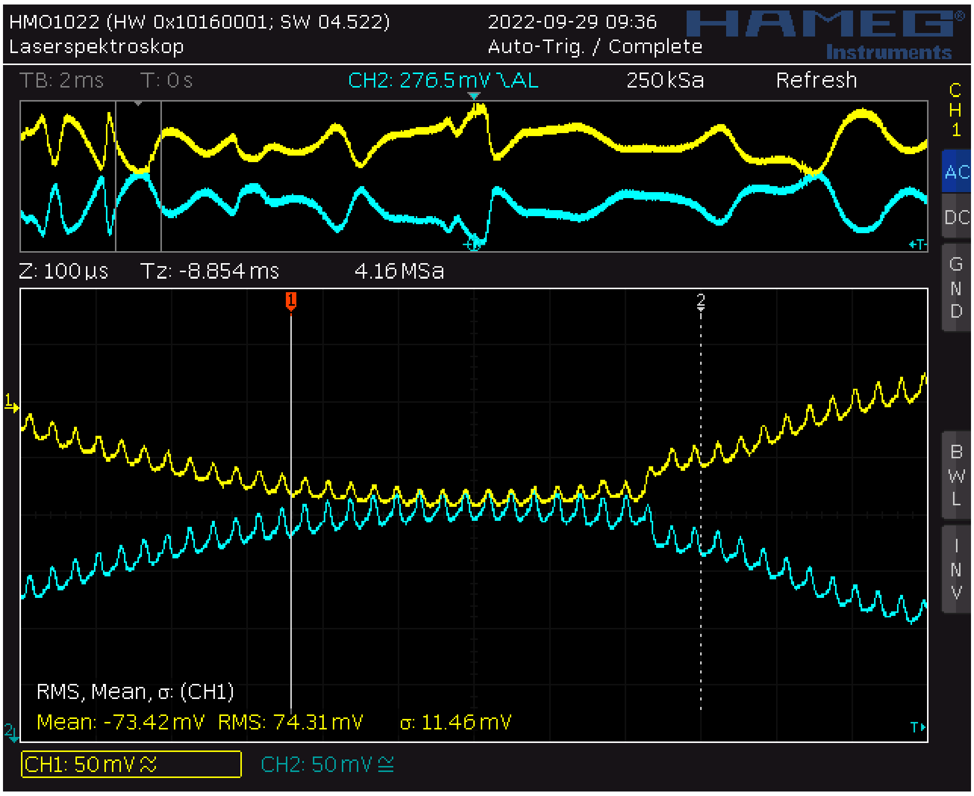

Figure 5: Output signals of diode D_1 and D_2 at the oscilloscope while tapping on the table. It can be seen that the signal is more or less noisy. The expected phase shift of 180° can already be seen.

frequency. It could be observed that the amplitude of the signals changed significantly depending on what frequency was played. A very good signal could be observed at around 717 Hz. This can be seen in fig. 6.

Here, the expected phase shift of 180° can be seen very well. It also did not change over time so that the setup could be expected to be calibrated properly.

After assuring the correct calibration of the setup, now the table was set to rotation. First different angular velocities were tried to see if everything works fine. There it could already be seen that the speed of the table sometimes varied or that the rotation suddenly stopped. To assure that the angular velocities were correct, a measurement was carried out for all possible speed settings, placing a smartphone on the table and measuring the angular velocity using the `phyphox` app. After the settings were adjusted, each time the measurement was started. Then the rotation was set to clockwise, after a short time interval to counterclockwise. It always had to be waited until the initial noise directly after starting the rotation disappeared. Also, some measurements had to be carried out several times, as the stepper motor did not always correspond in the right way to the preset values. Finally, it could be seen and heard from the sound of the motor that it was rotating faster at setting 18 than expected. This observation will also be analyzed later.

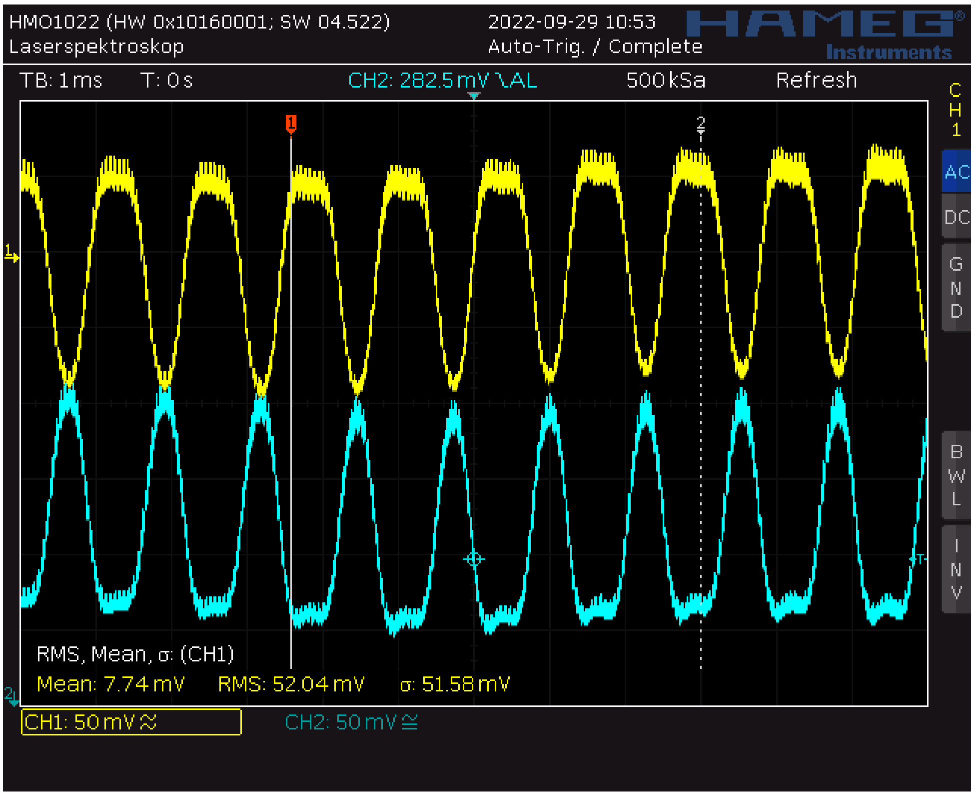

Figure 6: Output signals of diode D_1 and D_2 at the oscilloscope while playing a sound of 717 Hz on a smartphone placed on the turntable to achieve a stimulated vibration. The expected phase shift of 180° can be seen very well for the whole signal.

After having taken the data to calibrate the angular velocities, the measurements could be started. For all possible speed settings, the beat frequencies were noted. Again, it had to be waited until the rotation seemed to be stable until a constant frequency with minor fluctuations could be noted. As the fluctuations were very different in their amplitude, also the estimated uncertainties were noted for each setting.

To compare the results with theoretically expected values, the lengths of all sides were measured using a tape measure. For the whole area, also the height h perpendicular to the distance L_1 between M_1 and M_2 was measured.

4 Data Analysis

4.1 Calibration of the Turntable

As it could well be seen that the turntable did not always respond to the rotation setting in the same way, it was decided to perform a calibration using a smartphone gyroscope to measure the angular velocity of the table for each setting.

The smartphone was placed in the middle of the turntable and the data of the z-gyroscope was acquired using the `phyphox` app. For all possible speed settings, a measurement was taken, letting the table rotate clockwise first, then after a short break counterclockwise. It was always tried to wait until a clear signal with only small noise was visible, as lots of noise occurred directly after changing the speed. An example of a final signal can be seen in fig. 7. The fluctuations in amplitude directly after changing the setting can very well be seen.

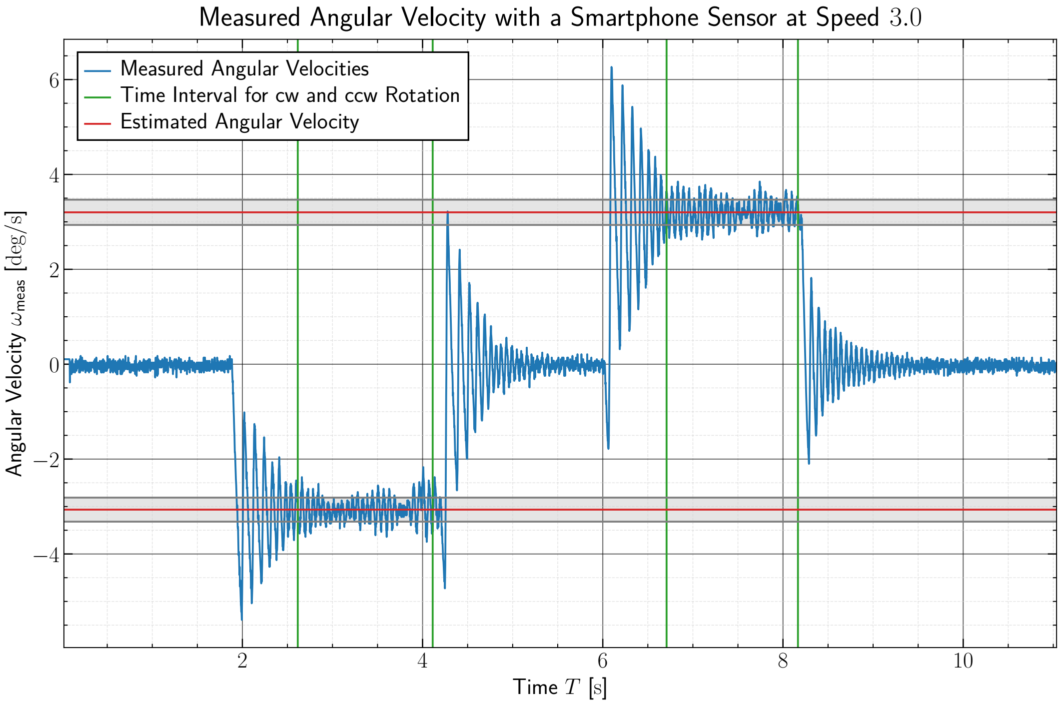

Figure 7: Angular velocities, measured with a smartphone sensor, using the `phyphox` app. The rotation speed of the table was set to 3.0, which corresponds to an angular velocity of (3.00 ± 0.02) deg/s, considering [1]. The green areas mark the time intervals were used for the analysis of the measured angular velocity. The first interval corresponds to a clockwise rotation of the table, the second interval to a counterclockwise rotation. The estimated values were calculated using eq. (12), taking the average over all values in the given interval. The corresponding standard deviation was used as the uncertainty.

The two green areas mark the time intervals used for the analysis of the angular velocity. The first interval corresponds to a clockwise rotation of the table, the second to a counterclockwise rotation. The intervals were estimated by hand to get as large time intervals as possible without considering the initial noise due to a changing of the settings.

To determine the angular velocity ω_{meas}, an average was calculated over all the values in the selected interval. The uncertainty was calculated using the standard deviation

$$\omega_{\text{meas}} = \frac{1}{n}\sum_{i=1}^{n}\omega_i \qquad \sigma_{\omega_{\text{meas}}} = \sqrt{\frac{1}{n-1}\sum_{i=1}^{n}\left(\omega_i - \omega_{\text{meas}}\right)^2}\,, \tag{12}$$

where $i \in [1, n]$ enumerates all the angular velocities in the selected time interval. The estimated values can be found in table 1.

To provide a conversion from settings to the measured angular velocity, a linear regression was performed. As described in [1], the settings do not correspond directly to the angular velocities ω_{set} of the table. The conversion can be found in [1] and in table 1. To estimate the conversion from the preset angular velocities ω_{set} to the measured velocities ω_{meas}, both were plotted in fig. 8 and a linear orthogonal distance regression was performed using `scipy.odr` to consider both x- and y- uncertainties.

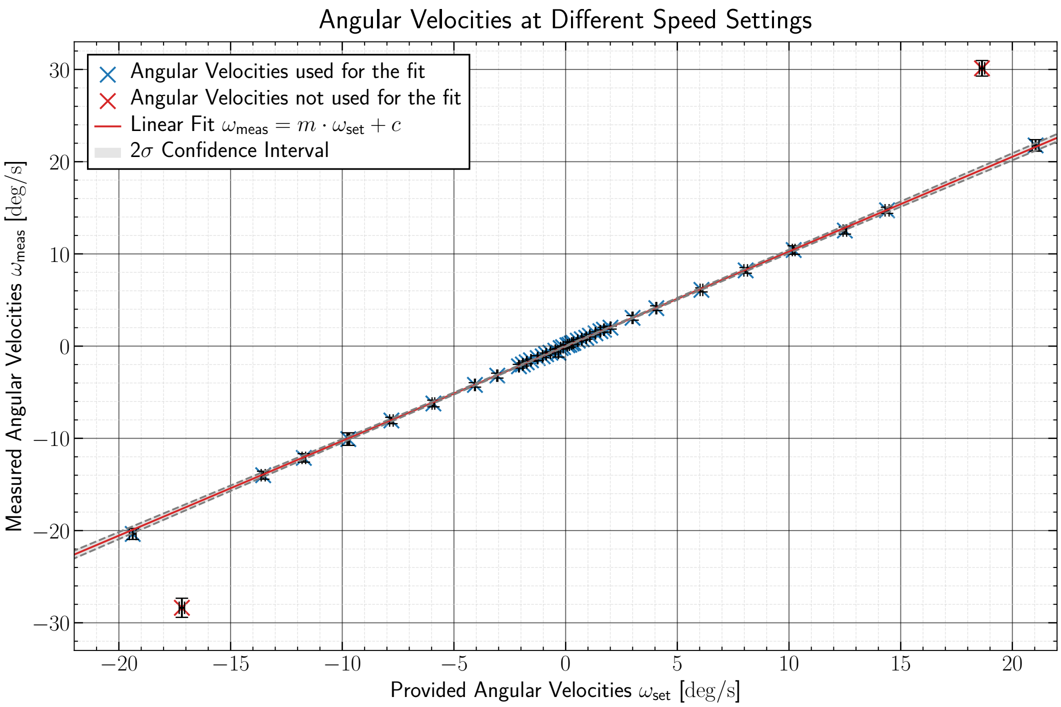

Figure 8: Measured angular velocities ω_{meas} at different speed settings. Considering [1], the speed settings correspond to the angular velocities ω_{set}. As the angular velocities for the speed setting 18 were obviously too high, this values were not used for further calibration. A linear orthogonal distance regression was performed using `scipy.odr` to consider the x- and y-uncertainties for the fit. The optimal fit parameters can be found in eq. (13). A list of the used settings and the corresponding calculated angular velocities ω_{cal} of the fit can be found in table 1.

As described in section 3, it could be heard and seen that the rotation speed of the turntable at setting 18 was much higher than expected, also much higher than for setting 20. As this great deviation from the expected velocity is also well visible in fig. 8 and table 1, it was decided not to use this value for the fit.

The model function

$$\omega_{\text{meas}} = m \cdot \omega_{\text{set}} + c \tag{13}$$

was used, as a linear correlation between the two angular velocities is expected. It provided the optimal values

$$m = (1.027 \pm 0.009) \tag{13a}$$
$$c = (-0.01 \pm 0.03)\,\mathrm{deg/s}\,. \tag{13b}$$

4.2 Analysis of the Beat Frequency

To verify the linear relationship between beat frequency and angular velocity described in eq. (9), the beat frequency was measured for different angular velocities.

The uncertainty on the frequency was estimated on basis of the fluctuations observed on the frequency counter. For clockwise rotation, the settings were taken as they were, and for counter clockwise rotation a negative sign was added. Using the phone data, the settings were converted to angular velocities as listed in table 1.

Then, three linear fits were performed. First, all frequencies measured at higher speeds of rotation were plotted against the angular velocities. The used data is listed in table 2, the plot is depicted in fig. 9. Then, for the lower frequencies, two separate plots were made for the clockwise and counterclockwise rotation. The data used for the clockwise and counterclockwise plots and the plots themselves are listed and shown in table 3 and fig. 10 and table 4 and fig. 11, respectively.

Then, a linear fit of the form

$$\Delta\nu_{\mathrm{rot}} = \alpha + \beta \cdot \omega \tag{14}$$

was performed. As due to the calibration with the smartphone there were uncertainties on both frequency and angular velocity, an orthogonal distance regression was performed using `scipy.odr` to consider the x- and y-uncertainties.

The fits are also visible in figs. 9 to 11 for the corresponding data sets. For each fit, the 2σ confidence interval is also drawn.

As for the data sets with lower angular velocity the lock-in effect can be seen, the lowest three data points, which clearly do not lie on a straight with the other points, were not used for the fit. They are marked in red.

For these data sets, the lock-in limits

$$\omega_{\mathrm{Lock}}^{\mathrm{cw}} = (0.31 \pm 0.04)\,\mathrm{deg/s} \qquad \omega_{\mathrm{Lock}}^{\mathrm{ccw}} = (0.41 \pm 0.07)\,\mathrm{deg/s}$$

were estimated by hand to be in between the data points that show the linear relationship and the data points that are obviously affected by the lock-in effect. As the lock-in limit is assumed to be between these points, the uncertainty was estimated to span both points. The estimated lock-in limits and their uncertainties are marked in orange in figs. 10 and 11.

The optimal parameters α_{h} and β_{h} for the high angular velocities, α_{cw} and β_{cw} for the clockwise rotation at low angular velocities and α_{ccw} and β_{ccw} for the counterclockwise

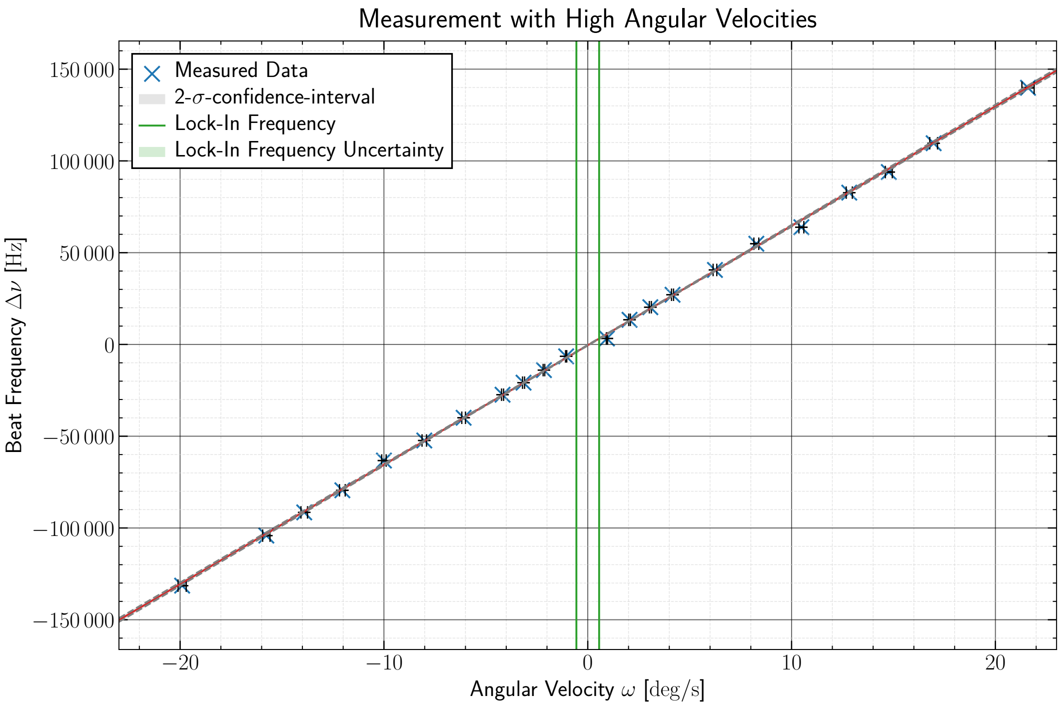

Figure 9: Beat frequencies $\Delta\nu$ plotted against the corresponding angular velocities ω for higher speeds of rotation (listed in table 2). To calculate the angular velocity from the turntable settings, the smartphone calibration listed in table 1 was used. As a linear relation is expected (described in eq. (9)), a linear fit of the from described in eq. (14) was performed using the orthogonal distance regression implemented in `scipy.odr`. The resulting parameters can be found in eq. (15). The lock-in limit calculated in section 4.2 is shown in green, the lock-in limit estimated from the measurement is shown in orange.

rotation at low angular velocities were calculated to.

$$\begin{aligned} \alpha_{\mathrm{h}} &= (-440 \pm 90)\,\mathrm{s}^{-1} & \beta_{\mathrm{h}} &= (6500 \pm 20)\,\mathrm{deg}^{-1} \\ \alpha_{\mathrm{cw}} &= (150 \pm 180)\,\mathrm{s}^{-1} & \beta_{\mathrm{cw}} &= (6560 \pm 140)\,\mathrm{deg}^{-1} \\ \alpha_{\mathrm{ccw}} &= (600 \pm 200)\,\mathrm{s}^{-1} & \beta_{\mathrm{ccw}} &= (6690 \pm 160)\,\mathrm{deg}^{-1}\,. \end{aligned} \tag{15}$$

The three side lengths of the gyroscope

$$L_1 = (42.5 \pm 0.5)\,\mathrm{cm} \qquad L_2 = (42.0 \pm 0.5)\,\mathrm{cm} \qquad L_1 = (41.5 \pm 0.5)\,\mathrm{cm}$$

as well as the height of triangle formed by the gyroscope $h = (36.5 \pm 0.5)\,\mathrm{cm}$ relative to L_1 were measured using a tape measure. The uncertainties were estimated, considering the fact that the tape measure had to be held above the setup. As the lengths differ, the setup could not be confirmed to form a equilateral triangle. Consequently, for the following calculations, the approximation of an equilateral triangle was not used.

The total path length of the beam is given by

$$L = L_1 + L_2 + L_3 \qquad s_L = \sqrt{(s_{L_1})^2 + (s_{L_2})^2 + (s_{L_3})^2}\,.$$

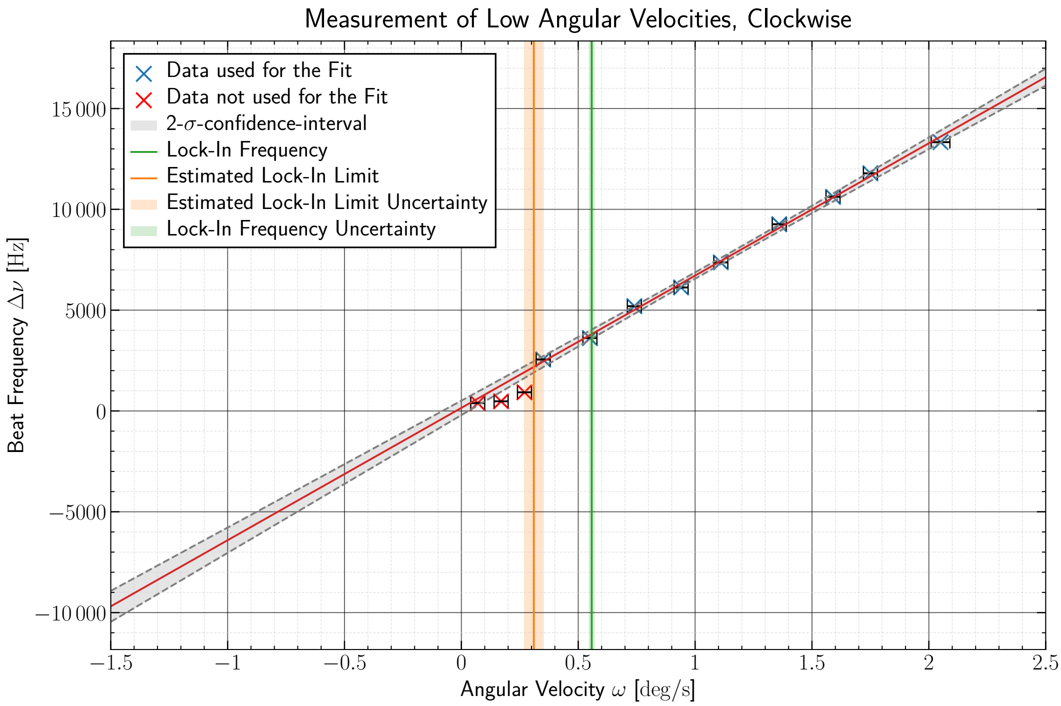

Figure 10: Beat frequencies $\Delta\nu$ plotted against the corresponding angular velocities ω for lower speeds of rotation with clockwise rotation (listed in table 3). To calculate the angular velocity from the turntable settings, the smartphone calibration listed in table 1 was used. As a linear relation is expected (described in eq. (9)), a linear fit of the from described in eq. (14) was performed using the orthogonal distance regression implemented in `scipy.odr`. The resulting parameters can be found in eq. (15). The data that was not used for the fit due to the lock-in effect is marked in red. The lock-in limit calculated in section 4.2 is shown in green, the lock-in limit estimated from the measurement is shown in orange.

From the geometric measurements, the area F enclosed by the light beam can be calculated

$$F = \frac{1}{2} \cdot L_1 \cdot h = (0.0776 \pm 0.0014)\,\mathrm{cm}^2\,.$$

The uncertainty is given by gaussian error propagation

$$s_F = \sqrt{\left(\frac{1}{2} \cdot L_1 \cdot s_h\right)^2 + \left(\frac{1}{2} \cdot h \cdot s_{L_1}\right)^2}\,. \tag{16}$$

Using eq. (9), the β-factor can be calculated from the geometric properties of the gyroscope. It is given by

$$\beta_{\text{theo}} = \frac{4 \cdot F}{L \cdot \lambda} = (6790 \pm 120)\,\mathrm{deg}^{-1}\,. \tag{17}$$

The uncertainty is given by

$$s_{\beta_{\text{theo}}} = \sqrt{\left(\frac{4 \cdot s_F}{L \cdot \lambda}\right)^2 + \left(\frac{4 \cdot F \cdot s_L}{L^2 \cdot \lambda}\right)^2}\,.$$

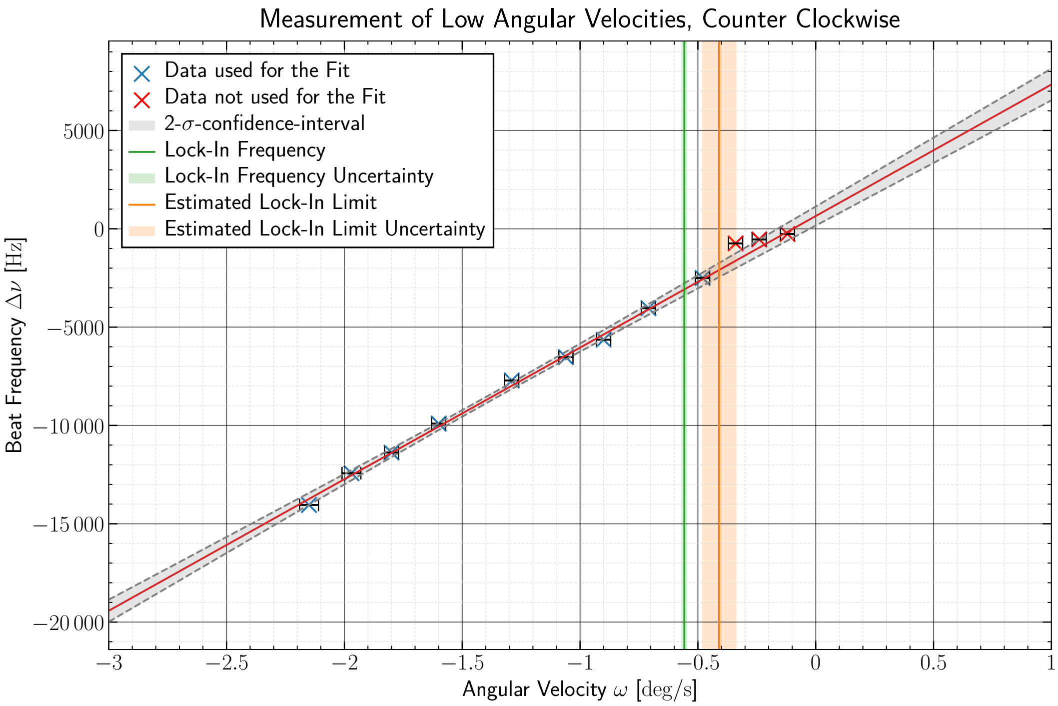

Figure 11: Beat frequencies $\Delta\nu$ plotted against the corresponding angular velocities ω for lower speeds of rotation with counterclockwise rotation (listed in table 4). To calculate the angular velocity from the turntable settings, the smartphone calibration listed in table 1 was used. As a linear relation is expected (described in eq. (9)), a linear fit of the from described in eq. (14) was performed using the orthogonal distance regression implemented in `scipy.odr`. The resulting parameters can be found in eq. (15). The data that was not used for the fit due to the lock-in effect is marked in red. The lock-in limit calculated in section 4.2 is also shown.

Additionally, using eq. (9), the wave length of the laser can be calculated from the path length L of the light, the area F the light beam encloses and the factor β from the fit by

$$\lambda = \frac{4 \cdot F}{L \cdot \beta} \qquad s_\lambda = \sqrt{\left(\frac{4 \cdot s_F}{L \cdot \beta}\right)^2 + \left(\frac{4 \cdot F \cdot s_L}{L^2 \cdot \beta}\right)^2 + \left(\frac{4 \cdot F \cdot s_\beta}{L \cdot \beta^2}\right)^2}\,, \tag{18}$$

where once again gaussian error propagation is used. For the higher angular velocities, lower angular velocities with clockwise rotation and lower angular velocities with counterclockwise rotation the wavelengths were calculated to

$$\lambda_\mathrm{h} = (660 \pm 12)\,\mathrm{nm}$$
$$\lambda_\mathrm{cw} = (654 \pm 19)\,\mathrm{nm}$$
$$\lambda_\mathrm{ccw} = (640 \pm 20)\,\mathrm{nm}\,,$$

respectively. These can be compared to the known wavelength of the HeNe laser later.

With eq. (11), the lock-in limit ω_Lock can theoretically be approximated to

$$\omega_\mathrm{Lock}^\mathrm{theo} = (0.558 \pm 0.010)\,\mathrm{deg/s}\,.$$

For this calculation, the literature wave length of a HeNe laser $\lambda_{\text{lit}} = 632.8\,\text{nm}$ was used. The uncertainty is given by gaussian error propagation

$$s_{\omega_{\text{Lock}}} = \sqrt{\left(\frac{c \cdot \lambda \cdot s_F}{8 \cdot \pi \cdot F^2} \cdot 10^{-4}\right)^2}.$$

The calculated lock-in limit is also shown in fig. 9, fig. 10 and fig. 11.

5 Summary and Discussion

In the first part of the experiment, the `phyphox` app was used to verify the turntable angular velocity settings. The results are listed in table 1.

As the correction factor of 1.027 ± 0.009 is only marginally higher than 1, it can be said that the correction factor is very small. However, as 1 is not within two standard deviations of the fit parameter, the regression definitely proves a deviation from the expected angular velocities, and the correction should be considered.

Especially noticeable was setting 18. While the angular velocity is listed as $(18.64 \pm 0.12)\,\mathrm{deg/s}$ for clockwise and $(-17.18 \pm 0.12)\,\mathrm{deg/s}$ for counterclockwise rotation in the manual [1], the phone measurements put the angular velocities at $\pm(28.4 \pm 1.0)\,\mathrm{deg/s}$. This unexpectedly high angular velocity was also observed directly. The turntable rotation at a setting of 18 was clearly higher than that at a setting 20.

A alsolso, it could be observed that often the turntable did not continuously rotate with a constant angular velocity, but would sometimes stop or randomly speed up.

Overall, the angular velocities provided in the manual [1] and the measured angular velocities lie within two standard deviations of one another, and therefore it can be said that they are compatible.

For further analysis, the calibration by the phone was used. As setting 18 is clearly not compatible with the other settings (see fig. 8), no beat frequencies were recorded for this setting.

For high angular velocities, low angular velocities with clockwise rotation and low angular velocities with counterclockwise rotation, the expected linear relationship described in eq. (9) could be verified. The scaling factors β_h, β_cw and β_ccw were determined using an orthogonal distance regression

$$\begin{aligned}\beta_\mathrm{h} &= (6500 \pm 20)\,\mathrm{deg}^{-1}\\ \beta_\mathrm{cw} &= (6560 \pm 140)\,\mathrm{deg}^{-1}\\ \beta_\mathrm{ccw} &= (6590 \pm 160)\,\mathrm{deg}^{-1}\,.\end{aligned}$$

The theoretical β factor was also calculated from eq. (9) to

$$\beta_\mathrm{theo} = (6790 \pm 120)\,\mathrm{deg}^{-1}\,.$$

This is within 2 to 3 standard deviations from all calculated β-factors. Therefore, it can be said that overall the calculated β factors match those theoretically predicted.

To take a possible systematic error into account, the fits were performed with a y-axis intercept

$$\begin{aligned} \alpha_{\mathrm{h}} &= (-440 \pm 90)\,\mathrm{s}^{-1} \\ \alpha_{\mathrm{cw}} &= (150 \pm 180)\,\mathrm{s}^{-1} \\ \alpha_{\mathrm{ccw}} &= (600 \pm 200)\,\mathrm{s}^{-1}\,. \end{aligned}$$

As the expected y-intercept of $0\,\mathrm{s}^{-1}$ is within 5, 1 and 3 standard deviations of the fit parameters, it is likely that no such systematic error was made.

The β-factors were used to calculate the wave lengths

$$\begin{aligned} \lambda_{\mathrm{h}} &= (660 \pm 12)\,\mathrm{nm} \\ \lambda_{\mathrm{cw}} &= (654 \pm 19)\,\mathrm{nm} \\ \lambda_{\mathrm{ccw}} &= (640 \pm 20)\,\mathrm{nm}\,. \end{aligned}$$

These are within 3, 2 and 1 standard deviations of the literature value of $632.8\,\mathrm{nm}$, which also indicates compatibility of measurement and theory.

Using section 4.2 and the literature value of $\lambda = 632.8\,\mathrm{nm}$ for the laser wave length, the lock-in limit was calculated to

$$\omega_{\mathrm{Lock}}^{\mathrm{theo}} = (0.558 \pm 0.010)\,\mathrm{deg/s}\,.$$

It can be seen alongside the data and the fits in figs. 9 to 11. For the frequencies measured at higher angular velocities, the lock-in limit is smaller than the angular velocities measured. This matches the measurement. For higher angular velocities, the lock-in effect is not visible in the data.

For lower angular velocities, the lock-in effect can be seen clearly. The lock-in limit was estimated to

$$\omega_{\mathrm{Lock}}^{\mathrm{cw}} = (0.31 \pm 0.04)\,\mathrm{deg/s} \qquad \omega_{\mathrm{Lock}}^{\mathrm{ccw}} = (0.41 \pm 0.07)\,\mathrm{deg/s}\,.$$

The calculated and estimated lock-in limits are shown in figs. 10 and 11 in green and orange, respectively. It is noticeable that the calculated lock-in limit is larger than the observed. Comparing $\omega_{\mathrm{Lock}}^{\mathrm{theo}}$ to $\omega_{\mathrm{Lock}}^{\mathrm{cw}}$ and $\omega_{\mathrm{Lock}}^{\mathrm{ccw}}$ yields a t-value of 6 and 2. Therefore, it can be said that the theoretically calculated value is compatible with the value measured for the counterclockwise rotation, but not with the value measured for the clockwise rotation. However, the compatibility $\omega_{\mathrm{Lock}}^{\mathrm{ccw}}$ and $\omega_{\mathrm{Lock}}^{\mathrm{theo}}$ mostly stems from the rather large estimated uncertainty of $\omega_{\mathrm{Lock}}^{\mathrm{ccw}}$, which was chosen due to a large distance between the data points. To gain meaningful results, measurements have to be made at smaller increments of the angular velocity.

The reason for the deviation of the calculated lock-in limit from the observed lock-in limit is most likely the approximations used in calculating the lock-in limit. For the calculation in section 4.2, the worst case, a phase angle between back-scattered and resonator wave of $\gamma = 0°$, is assumed. The measured data puts the lock-in limit at vastly lower values. Therefore, it can be assumed that the actual angle γ was high enough that the approximation does not hold true for the setup in this experiment.

A Appendix

List of Figures

List of Tables

Bibliography

[1] *Laser Education Kit CA-1310 Laser Gyroscope*. eLas, Diezenthalweg 8, 79426 Buggingen, Germany, 2016, Sept. 30, 2022.

[2] Dr. Walter Luhs. *LM-0600 HeNe Laser Gyroscope*. Photinik Ingenieurbüro, 2018, Sept. 30, 2022.

[3] Mira Naftaly. *Mode Locking in the Ring Laser Gyroscope: Reduced Treshold for the Two Cavity Modes*. Department of Physics, BruneI University, September 1990, Sept. 30, 2022.

Experimental Setup

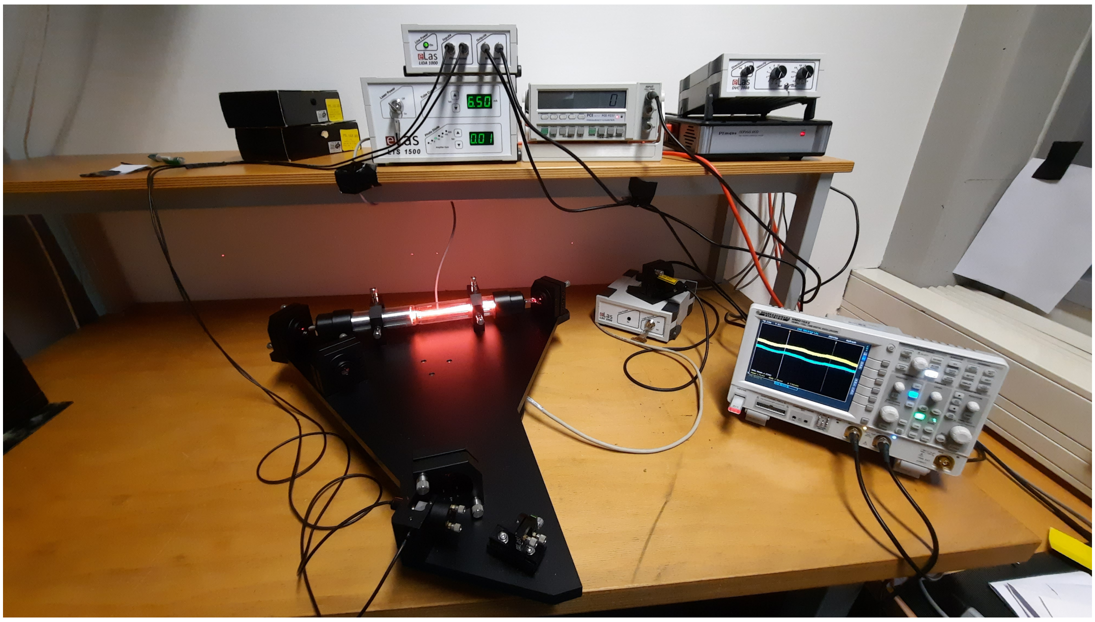

Figure 12: Setup used for this experiment. In the middle, the turntable and the laser can be seen. At the top, the laser supply, frequency counter and the rotation stage for the stepper motor can be seen. The oscilloscope at the right was used to show the output of both photo diodes and check their phase shift.

Figure 13: Setup of the optical axis. The HeNe-tube can be seen at the top as well as the three mirrors at the corners. On the left side between the two mirrors, the Single-Mode-Etalon can be found. At the front, the beam splitter and the two photo diodes can be seen.

Calibration of the Setup

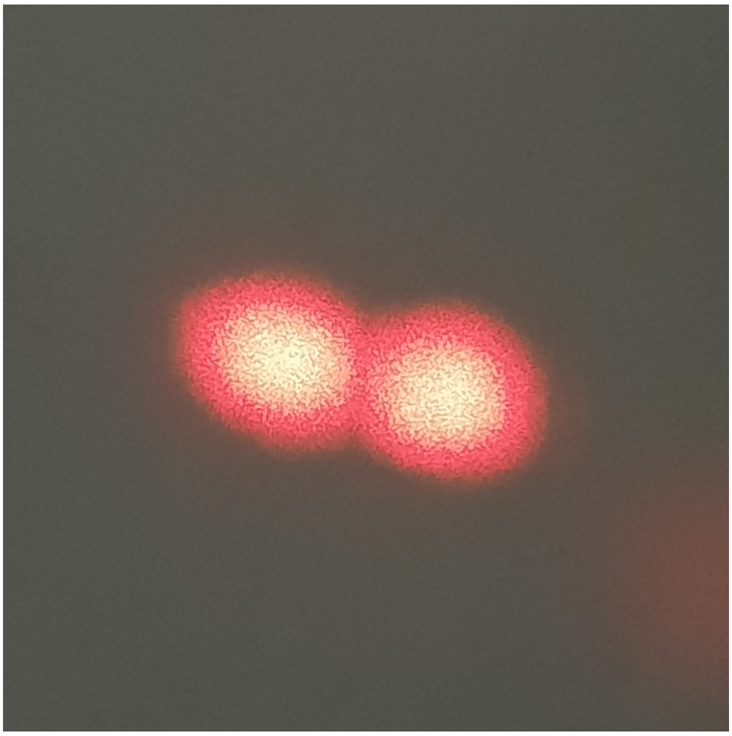

Figure 14: Laser point 3 m after diode D_2 before final calibration of the experimental setup.

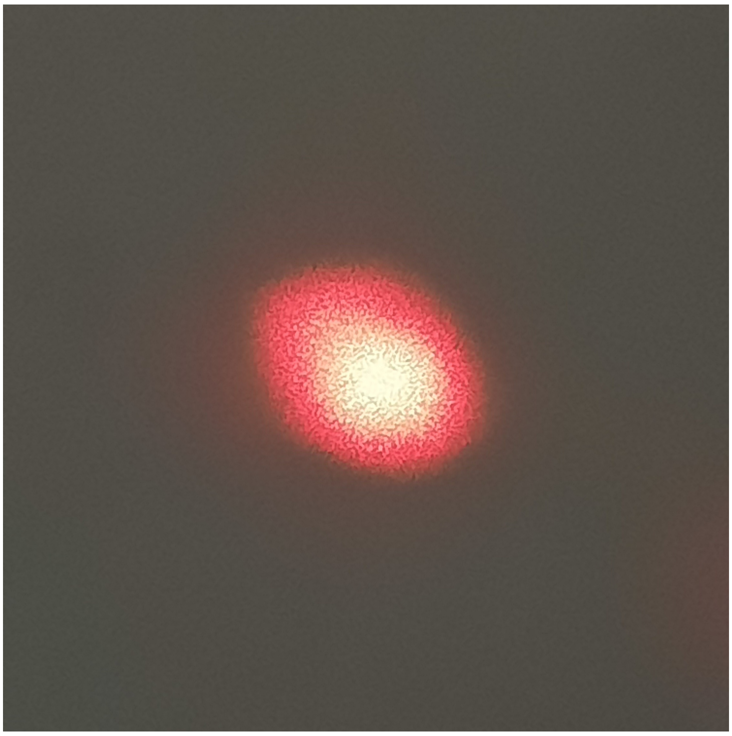

Figure 15: Laser point 3 m after diode D_2 after final calibration of the experimental setup.

Smartphone Data used to Measure the Angular Velocities

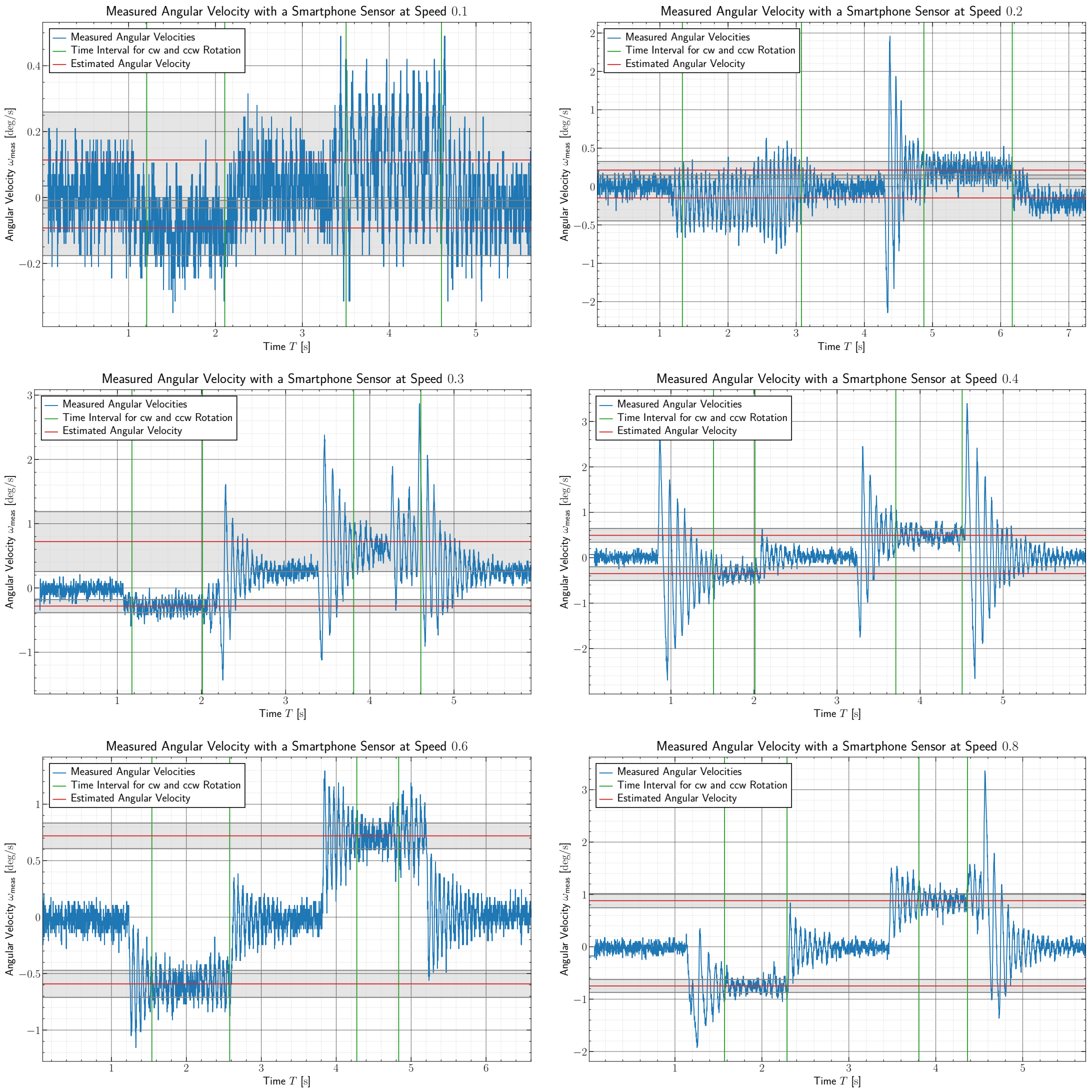

Figure 16: Angular velocities, measured with a smartphone sensor, using the `phyphox` app. The rotation speed was set to values from 0.1 to 1.2. The corresponding angular velocities of the table can be found in [1] and table 1. The green areas mark the time intervals, which were used for the analysis of the measured angular velocity. The first interval corresponds to a clockwise rotation of the table, the second interval to a counterclockwise rotation. The estimated values were calculated using eq. (12), taking the average over all values in the given interval. The uncertainty was calculated as the corresponding standard deviation.

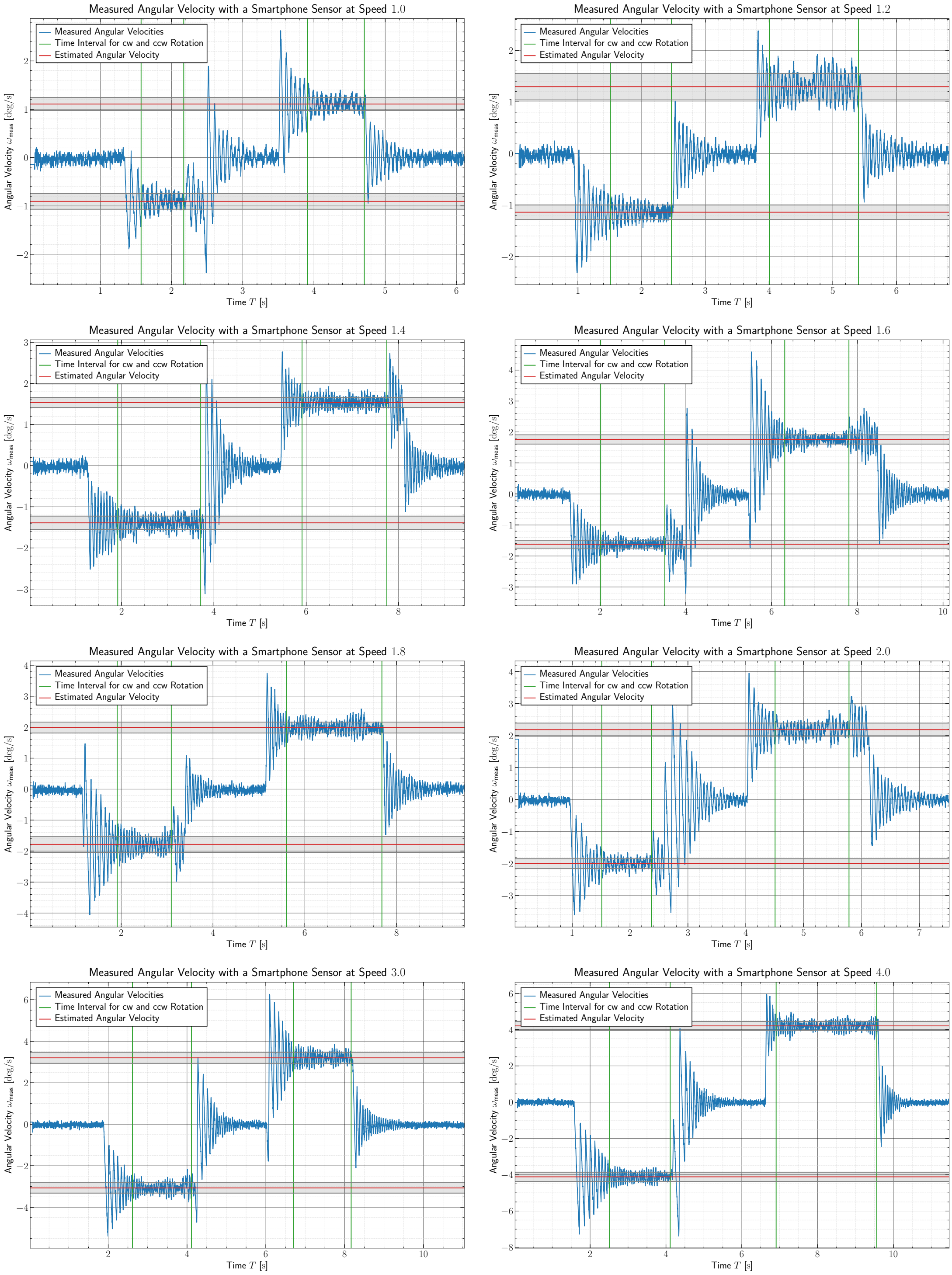

Figure 17: Angular velocities, measured with a smartphone sensor, using the `phyphox` app. The rotation speed was set to values from 1.4 to 8.0. The corresponding angular velocities of the table can be found in [1] and table 1. The green areas mark the time intervals, which were used for the analysis of the measured angular velocity. The first interval corresponds to a clockwise rotation of the table, the second interval to a counterclockwise rotation. The estimated values were calculated using eq. (12), taking the average over all values in the given interval. The uncertainty was calculated as the corresponding standard deviation.

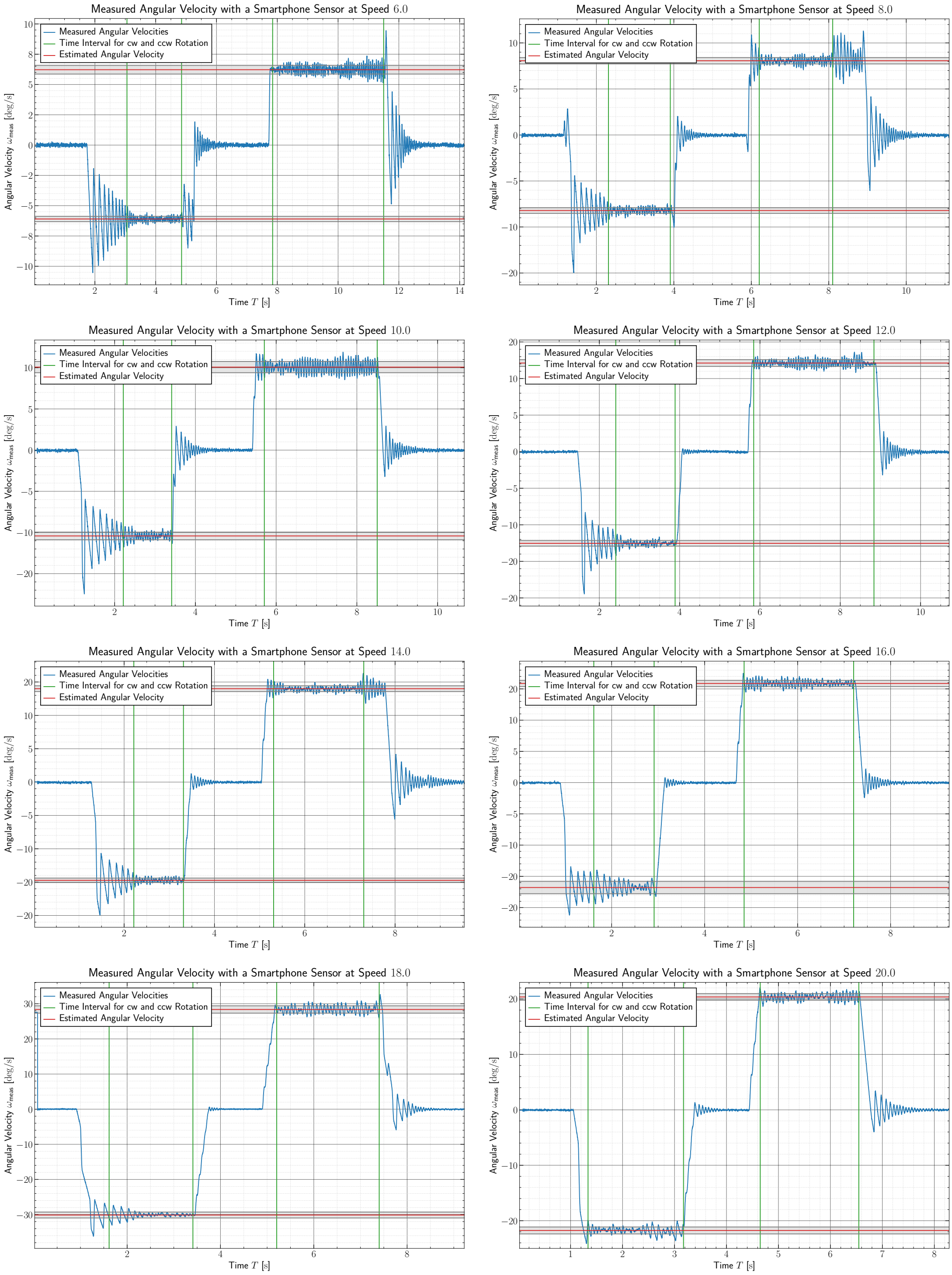

Figure 18: Angular velocities, measured with a smartphone sensor, using the `phyphox` app. The rotation speed was set to values from 10.0 to 20.0. The corresponding angular velocities of the table can be found in [1] and table 1. The green areas mark the time intervals, which were used for the analysis of the measured angular velocity. The first interval corresponds to a clockwise rotation of the table, the second interval to a counterclockwise rotation. The estimated values were calculated using eq. (12), taking the average over all values in the given interval. The uncertainty was calculated as the corresponding standard deviation.

Conversion from Settings to the Angular Velocities

Setting [a.u.]	ω_{set} [deg/s]	ω_{cal} [deg/s]	ω_{meas} [deg/s]
−20.0	−19.38 ± 0.15	−19.9 ± 0.2	−20.4 ± 0.6
−18.0	−17.18 ± 0.12	−17.6 ± 0.2	−28.4 ± 1.0
−16.0	−15.35 ± 0.10	−15.77 ± 0.18	−15.9 ± 0.5
−14.0	−13.54 ± 0.09	−13.91 ± 0.16	−14.0 ± 0.4
−12.0	−11.72 ± 0.08	−12.04 ± 0.14	−12.1 ± 0.5
−10.0	−9.73 ± 0.06	−10.00 ± 0.11	−10.1 ± 0.7
−8.0	−7.80 ± 0.08	−8.02 ± 0.11	−8.1 ± 0.3
−6.0	−5.92 ± 0.06	−6.09 ± 0.09	−6.2 ± 0.4
−4.0	−4.06 ± 0.02	−4.18 ± 0.05	−4.2 ± 0.2
−3.0	−3.06 ± 0.02	−3.15 ± 0.05	−3.2 ± 0.3
−2.0	−2.089 ± 0.016	−2.15 ± 0.04	−2.2 ± 0.2
−1.8	−1.915 ± 0.014	−1.97 ± 0.04	−1.99 ± 0.18
−1.6	−1.741 ± 0.012	−1.80 ± 0.03	−1.76 ± 0.15
−1.4	−1.552 ± 0.010	−1.60 ± 0.03	−1.53 ± 0.12
−1.2	−1.249 ± 0.010	−1.29 ± 0.03	−1.3 ± 0.3
−1.0	−1.027 ± 0.009	−1.06 ± 0.03	−1.11 ± 0.14
−0.8	−0.874 ± 0.008	−0.90 ± 0.03	−0.88 ± 0.13
−0.6	−0.680 ± 0.007	−0.71 ± 0.03	−0.72 ± 0.11
−0.4	−0.462 ± 0.006	−0.48 ± 0.03	−0.49 ± 0.15
−0.3	−0.324 ± 0.004	−0.34 ± 0.03	−0.7 ± 0.5
−0.2	−0.223 ± 0.003	−0.24 ± 0.03	−0.21 ± 0.11
−0.1	−0.114 ± 0.002	−0.12 ± 0.03	−0.11 ± 0.15
0.1	0.078 ± 0.002	0.07 ± 0.03	0.11 ± 0.15
0.2	0.169 ± 0.003	0.17 ± 0.03	0.21 ± 0.11
0.3	0.269 ± 0.004	0.27 ± 0.03	0.7 ± 0.5
0.4	0.348 ± 0.006	0.35 ± 0.03	0.49 ± 0.15
0.6	0.545 ± 0.007	0.55 ± 0.03	0.72 ± 0.11
0.8	0.724 ± 0.008	0.74 ± 0.03	0.88 ± 0.13
1.0	0.922 ± 0.009	0.94 ± 0.03	1.11 ± 0.14
1.2	1.085 ± 0.010	1.11 ± 0.03	1.3 ± 0.3
1.4	1.334 ± 0.010	1.36 ± 0.03	1.53 ± 0.12
1.6	1.556 ± 0.012	1.59 ± 0.03	1.76 ± 0.15
1.8	1.716 ± 0.014	1.75 ± 0.03	1.99 ± 0.18
2.0	2.008 ± 0.016	2.05 ± 0.04	2.2 ± 0.2
3.0	3.00 ± 0.02	3.07 ± 0.05	3.2 ± 0.3
4.0	4.06 ± 0.02	4.16 ± 0.05	4.2 ± 0.2
6.0	6.08 ± 0.06	6.24 ± 0.09	6.2 ± 0.4
8.0	8.06 ± 0.08	8.27 ± 0.12	8.1 ± 0.3
10.0	10.21 ± 0.06	10.48 ± 0.12	10.1 ± 0.7
12.0	12.50 ± 0.08	12.83 ± 0.15	12.1 ± 0.5
14.0	14.39 ± 0.09	14.77 ± 0.17	14.0 ± 0.4
16.0	16.53 ± 0.10	16.97 ± 0.19	15.9 ± 0.5
18.0	18.64 ± 0.12	19.1 ± 0.2	28.4 ± 1.0
20.0	21.04 ± 0.15	21.6 ± 0.3	20.4 ± 0.6

Table 1: Conversion from the used settings of the rotating table to the corresponding angular velocities. ω_{set} is the angular velocity in deg/s corresponding to the preset speed. The conversion can be taken from [1]. The calculated angular velocity ω_{cal} was estimated using a linear regression visible in fig. 8 and eq. (13). The measured angular velocities ω_{meas} were calculated as the average value over the corresponding time intervals, using eq. (12). The data used to estimate ω_{meas} is visible in figs. 16 to 18 in appendix A.

Beat frequencies measured at different angular velocities

Setting	Angular Velocity ω [deg/s]	Beat Frequency [Hz]
−20.0	−19.9 ± 0.2	−131 400 ± 600
−16.0	−15.77 ± 0.18	−104 100 ± 600
−14.0	−13.91 ± 0.16	−91 500 ± 400
−12.0	−12.04 ± 0.14	−79 500 ± 1700
−10.0	−10.00 ± 0.11	−63 000 ± 2000
−8.0	−8.02 ± 0.11	−52 330 ± 100
−6.0	−6.09 ± 0.09	−39 940 ± 80
−4.0	−4.18 ± 0.05	−27 380 ± 70
−3.0	−3.15 ± 0.05	−20 820 ± 40
−2.0	−2.15 ± 0.04	−13 970 ± 70
−1.0	−1.06 ± 0.03	−6470 ± 60
1.0	0.94 ± 0.03	3250 ± 100
2.0	2.05 ± 0.04	13 430 ± 40
3.0	3.07 ± 0.05	20 290 ± 30
4.0	4.16 ± 0.05	27 080 ± 50
6.0	6.24 ± 0.09	40 590 ± 70
8.0	8.27 ± 0.12	54 900 ± 200
10.0	10.48 ± 0.12	64 000 ± 4000
12.0	12.83 ± 0.15	82 700 ± 1200
14.0	14.77 ± 0.17	93 900 ± 800
16.0	16.97 ± 0.19	109 600 ± 400
20.0	21.6 ± 0.3	139 900 ± 1200

Table 2: Beat frequencies measured at high angular velocities, used for the fit in fig. 9.

Setting	Angular Velocity ω [deg/s]	Beat Frequency [Hz]
0.1	0.07 ± 0.03	400 ± 500
0.2	0.17 ± 0.03	500 ± 200
0.3	0.27 ± 0.03	900 ± 300
0.4	0.35 ± 0.03	2550 ± 100
0.6	0.55 ± 0.03	3620 ± 70
0.8	0.74 ± 0.03	5200 ± 150
1.0	0.94 ± 0.03	6130 ± 100
1.2	1.11 ± 0.03	7400 ± 200
1.4	1.36 ± 0.03	9300 ± 200
1.6	1.59 ± 0.03	10 620 ± 40
1.8	1.75 ± 0.03	11 790 ± 80
2.0	2.05 ± 0.04	13 330 ± 80

Table 3: Beat frequencies measured at low angular velocities at clockwise rotation, used for the fit in fig. 10.

Setting	Angular Velocity ω [deg/s]	Beat Frequency [Hz]
-2.0	-2.15 ± 0.04	$-14\,040 \pm 80$
-1.8	-1.97 ± 0.04	$-12\,430 \pm 50$
-1.6	-1.80 ± 0.03	$-11\,380 \pm 40$
-1.4	-1.60 ± 0.03	-9910 ± 80
-1.2	-1.29 ± 0.03	-7710 ± 120
-1.0	-1.06 ± 0.03	-6530 ± 120
-0.8	-0.90 ± 0.03	-5640 ± 70
-0.6	-0.71 ± 0.03	-4000 ± 200
-0.4	-0.48 ± 0.03	-2500 ± 300
-0.3	-0.34 ± 0.03	-700 ± 300
-0.2	-0.24 ± 0.03	-500 ± 300
-0.1	-0.12 ± 0.03	-300 ± 400

Table 4: Beat frequencies measured at low angular velocities at counterclockwise rotation, used for the fit in fig. 11.

A.1 Lab Notes

Laser gyroscope 29.09.22 - 30.09.22

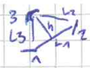

42,5

mirror 1 - 2 : L_1 = (~~[illegible]~~ ± 0,5) cm

mirror 2 - 3 : L_2 = (42,0 ± 0,5) cm

mirror 1 - 3 : L_3 = (41,5 ± 0,5) cm

h = (36,5 ± 0,5) cm

measurement 1

cw: speed [deg/s]	frequency [Hz]	ccw: speed [deg/s]	frequency [Hz]
1,0	6231	1,0	6566
2,0	14315	2,0	14024
3,0	20769	3,0	20644
4,0	27081	4,0	27348
6,0	40393	6,0	40088
8,0	53859	8,0	52678
10,0	68098	10,0	65801
12,0	81653	12,0	78675
14,0	96631	14,0	97134
16,0	110163	16,0	103814
18,0			
20,0	140059		131134

etalon

speed	frequency	speed	frequency
2,0	13455	2,0	13704
1,8	11810	1,8	12422
1,6	10613	1,6	11327
1,4	9302	1,4	9805
1,2	7399	1,2	7967
1,0	6020	1,0	6285
0,8	5029	0,8	5242
0,6	3435	0,6	3433
0,4	~~[illegible]~~ 2610	0,4	2636
0,3	1321	0,3	1649
0,2	1193	0,2	1142
0,1	646	0,1	792

measurement 2

speed	frequency	speed	frequency
1,0	6250 ± 100	1,0	6472 ± 60
2,0	~~[illegible]~~ 13426 ± 40	2,0	13970 ± 70
3,0	20292 ± 30	3,0	20820 ± 40
~~4,0~~	~~[illegible]~~		
4,0	27078 ± 50	4,0	27380 ± 70
6,0	40593 ± 70	6,0	39945 ± 80
8,0	54882 ± 200	8,0	52332 ± 100
10,0	63879 ± 3500	10,0	63258 ± 2000
12,0	82720 ± 1200	12,0	79466 ± 1700
14,0	93937 ± 800	14,0	91505 ± 400
16,0	109632 ± 400	16,0	104149 ± 600
20,0	139861 ± 1200	20,0	131417 ± 600
2,0	13332 ± 80	2,0	14044 ± 80
1,8	11789 ± 80	1,8	12430 ± 50
1,6	10621 ± 40	1,6	11376 ± 40
1,4	9261 ± 200	1,4	9906 ± 80
1,2	7368 ± 200	1,2	7712 ± 120
1,0	6127 ± 100	1,0	6528 ± 120
0,8	5198 ± 150	0,8	5641 ± 70
0,6	3615 ± 70	0,6	4036 ± 200
0,4	2554 ± 100	0,4	2504 ± 300
0,3	926 ± 300	0,3	742 ± 300
0,2	478 ± 200	0,2	540 ± 300
0,1	389 ± 500	0,1	263 ± 400